Binuclear Cu_A Formation in Biosynthetic Models of Cu_A in Azurin Proceeds via a Novel Cu(Cys)₂His Mononuclear Copper Intermediate

Saumen Chakraborty,^{†,§} Michael J. Polen,^{†,±} Kelly N. Chacón,^{‡,⊥} Tiffany D. Wilson,[†] Yang Yu,^{†,≠} Julian Reed,[†] Mark J. Nilges,[†] Ninian J. Blackburn,^{‡,*} Yi Lu^{†,*}

† Department of Chemistry, University of Illinois at Urbana-Champaign, Urbana, IL 61801, USA ‡ Institute of Environmental Health, Oregon Health & Sciences University, Portland, OR 97239, USA

Email: yi-lu@illinois.edu; blackbni@ohsu.edu

Abstract

 Cu_A is a binuclear electron transfer (ET) center found in cytochrome c oxidases (CcOs), nitrous oxide reductases (N2ORs), and nitric oxide reductase (NOR). In these proteins, the Cu_A centers facilitate efficient ET ($k_{ET} > 10^4 \text{ s}^{-1}$) under low thermodynamic driving forces (10-90 mV). While the structure and functional properties of CuA are well understood, a detailed mechanism of copper incorporation into the protein and the identity of the intermediates formed during the Cu_A maturation process are still lacking. Previous studies of the Cu_A assembly mechanism in vitro using a biosynthetic model Cu_A center in azurin (Cu_AAz) identified a novel intermediate X (I_x) during reconstitution of the binuclear site. However, due to the instability of Ix and the coexistence of other Cu centers, such as CuA' and type 1 copper centers, the identity of this intermediate could not be established. Here, we report the mechanism of CuA assembly using variants of Glu114XCuAAz (X=Gly, Ala, Leu, Gln), the backbone carbonyl of which acts as a ligand to the Cu_A site, with a major focus on characterization of the novel intermediate I_x. We show that Cu_A assembly in these variants proceeds through several types of Cu centers, such as mononuclear red type 2 Cu, the novel intermediate lx, and blue type 1 Cu. Our results show that the backbone flexibility of the Glu114 residue is an important factor in determining the rates of T2Cu→I_x formation, suggesting that the Cu_A formation is facilitated by swinging of the ligand loop, which internalizes the T2Cu capture complex to the protein interior. The kinetic data further suggests that the nature of the Glu114 side chain influences the timescales on which these intermediates are formed, the wavelengths of the absorption peaks, and how cleanly one intermediate is converted to another. Through careful understanding of these mechanism and optimization of the conditions, we have obtained I_x in ~80-85% population in these variants, which allowed us to employ UV-Vis, EPR, and EXAFS spectroscopic techniques to identify the Ix as a mononuclear Cu(Cys)2(His) complex. Since some of the intermediates have been proposed to be involved in the assembly of native CuA, these results shed light on the structural features of the important intermediates and mechanism of Cu_A formation.

Introduction

Electron transfer (ET) is essential for many biological processes, such as photosynthesis, respiration, and dinitrogen fixation.¹ To facilitate these processes, copper proteins involved in redox and ET process, called cupredoxins, are often utilized, and they share a common Greek-key-β-barrel fold, where the majority of copper-coordinating ligands occur in a loop.²⁻⁹ A Cys thiolate is a ligand common in cupredoxins, which makes these proteins intense in color, due to S_{Cys}→Cu charge transfer (CT) transitions. Three types of copper sites are typically found in cupredoxins: the blue mononuclear type 1 copper (T1Cu) with distorted trigonal geometry, the red mononuclear type 2 copper (T2Cu) with square pyramidal geometry, and the purple binuclear Cu_A with a diamond core geometry.^{3, 10-12} While the T1Cu and Cu_A sites facilitate ET, the T2Cu sites are generally involved in catalysis.¹⁰

One important class of these copper sites is the binuclear purple CuA, which is found in enzymes involved in aerobic and anaerobic respiration, such as cytochrome c oxidases (CcOs), 13-15 quinol oxidase (SoxH), 16, 17 nitrous oxide reductases (N2ORs), 18, 19 and nitric oxide reductase (qCuANOR).²⁰ In these proteins, the CuA site acts as a terminal ET center by accepting electrons from donors, such as cytochromes c, and transferring them to redox partners with high efficiency (e.g. ET rate, $k_{ET} > 10^4$ s⁻¹), despite low thermodynamic driving forces (10-90 mV) for such ET. The Cu_A centers are characterized by a mixed valence [Cu^(+1.5)-Cu^(+1.5)] site, containing a weak Cu-Cu bond. in which one electron is delocalized between the two copper ions.²¹⁻²³ The two copper ions are coordinated by two Cys residues to form a rigid "diamond" core, and each metal ion is also coordinated by a His residue (Fig. 1A). These structural features of the Cu_A site also bestow them with unique spectroscopic signatures. The UV-vis of Cu_A sites have two $S_{Cys} \rightarrow Cu(II)$ CT at ~480 and 530 nm (ε ~3000-4000 M⁻¹cm⁻¹), and a broad peak due to a Cu-based ($\psi \rightarrow \psi^*$) transition centered at ~800 nm (ϵ ~2000 M⁻¹cm⁻¹), giving the Cu_A a strong purple color. 16, 21, 24-27 The electron paramagnetic resonance (EPR) spectrum consists of a seven line hyperfine splitting pattern due to valence delocalization of the unpaired d electron between the two Cu nuclei, each having a nuclear spin $I = 3/2.^{22}$ On the other hand, the T1Cu center also displays intense blue color, due to strong absorbance at ~600 nm (ε ~2000-6000 M⁻¹cm⁻¹) that arises from $S_{Cvs}(\pi) \rightarrow Cu(II)$ CT transition. It also differs from the typical T2 Cu center by a small 4-line EPR hyperfine splitting pattern, which is due to valence delocalization of the unpaired d electron onto the mononuclear Cu. In general, the CuA center displays even smaller hyperfine splitting ($A_z \sim 30-40 \times 10^{-4} \text{ cm}^{-1}$) than T1Cu site ($A_z \sim 30-90 \times 10^{-4} \text{ cm}^{-1}$) than T1Cu site ($A_z \sim 30-90 \times 10^{-4} \text{ cm}^{-1}$) 10⁻⁴ cm⁻¹) as the hyperfine splitting is divided into two copper atoms.¹⁰ The red T2Cu center, in contrast, exhibits an intense absorption ~360-400 nm, due to a $S_{Cys}(\sigma) \rightarrow Cu(II)$ CT transition. It also displays 4-line EPR hyperfine splitting pattern with a much larger hyperfine splitting ($A_z \sim 130\text{-}180 \text{ x } 10^{-4} \text{ cm}^{-1}$) than those in Cu_A or T1Cu centers, reflecting a lesser extent of covalency.^{28, 29} From phylogenetic and sequence analyses, it has been suggested that the blue T1Cu, red T2Cu, and purple Cu_A sites have evolved from a common ancestor.³⁰ All three types of Cu centers were observed in a study involving *in vitro* reconstitution of the Cu_A site of N₂OR from *Paracoccus denitrificans*.³¹

Due to the presence of multiple cofactors in the proteins containing Cu_A centers (hemes in CcOs and qCu_ANOR, tetranuclear Cu_Z in N₂ORs), studying the Cu_A sites in these proteins has been hindered by intense and overlapping spectral features.^{16, 17, 19, 20} One strategy that has been employed to study Cu_A sites involves expressing the soluble Cu_A domain from CcO and reconstituting the Cu_A site *in vitro*.^{16, 25-27, 32-36} In a second strategy the Cu_A ligands have been engineered in another cupredoxin protein followed by *in vitro* reconstitution of the binuclear site.³⁷⁻⁴⁰ By replacing the Cu binding loop from T1Cu proteins with the Cu_A loop from CcO, the Cu_A site was successfully engineered into CyoA domain of a copper-less quinol oxidase (called Cu_A-CyoA) and blue T1Cu proteins amicyanin (called Cu_AAmi) and azurin (Az, called Cu_AAz).^{38,37, 40-44}

While the Cu_A center has been well studied, one of the remaining challenges in understanding this class of copper center is the mechanism of its formation, particularly how the mixed valence species [Cu^(+1.5)-Cu^(+1.5)] is formed from either Cu(I) or Cu(II) ions. The red T2Cu Sco1 protein from the inner mitochondrial membrane, which exhibits Cu(Cys)₂His ligation, has been implicated to be the chaperone responsible for Cu delivery to the Cu_A site. ⁴⁵⁻⁵⁰ Quite interestingly, binding of both Cu(II) and Cu(I) to Sco1 has been proposed to be important for normal functioning of this protein. ⁵¹⁻⁵³ Alternatively, it has been proposed that Sco1 acts as disulfide reductase to keep the active site Cys of Cu_A in the reduced state or to maintain a proper redox buffering of metal ions. The latter inference stems from the fact that Sco1 possesses the thioredoxin fold. ^{50, 54, 55} In *Bacillus subtilis*, another protein, YpmQ, which is the yeast homologue of Sco1, and has a Cu(Cys)₂His ligation, has also been proposed to be required for Cu_A assembly. Furthermore, the periplasmic protein PCu_AC, found in several prokaryotes has been shown to deliver Cu(I) to apo Cu_A, forming the binuclear Cu(I)-Cu_A site. ⁵⁴

In order to gain insight into Cu_A assembly, studies have been undertaken using both soluble domain of *Thermus thermophilus (Tt)* Cu_A^{56, 57} and biosynthetic models of Cu_A in azurin (called Cu_AAz).^{58, 59} A single intermediate was observed as a rapidly-formed green Cu center in the soluble domain of *Tt* Cu_A and this intermediate was identified as a mononuclear Cu(II)(Cys)₂(His) complex, based on UV-vis, EPR and X-ray absorption spectroscopy (XAS) studies.⁵⁶ On the other hand, addition of 10-fold excess CuSO₄ to the apo Cu_AAz, a red T2Cu intermediate was formed within 10 ms, followed by formation of the purple Cu_A site at longer times.⁵⁸ Recently, it has been shown that under sub-equivalent Cu(II) addition, the formation of binuclear Cu_A center is an intricate

process, such that in addition to the formation of the red T2Cu intermediate, a novel green copper intermediate, I_x, and a blue T1Cu intermediate was observed prior to Cu_A formation.⁵⁹ The proposed mechanism invoked the formation of an initial red T2Cu involving Cys116 that is close to the protein exterior. The next step of the kinetic process is then branched into a) the formation of binuclear Cu_A', a Cu_A lacking His120 ligation, and b) a conformational change of the metal binding loop, leading to reorientation of the capture complex toward the protein interior and accompanying ligation by Cys112 and His46, forming I_x. Through comparison to the spectral properties

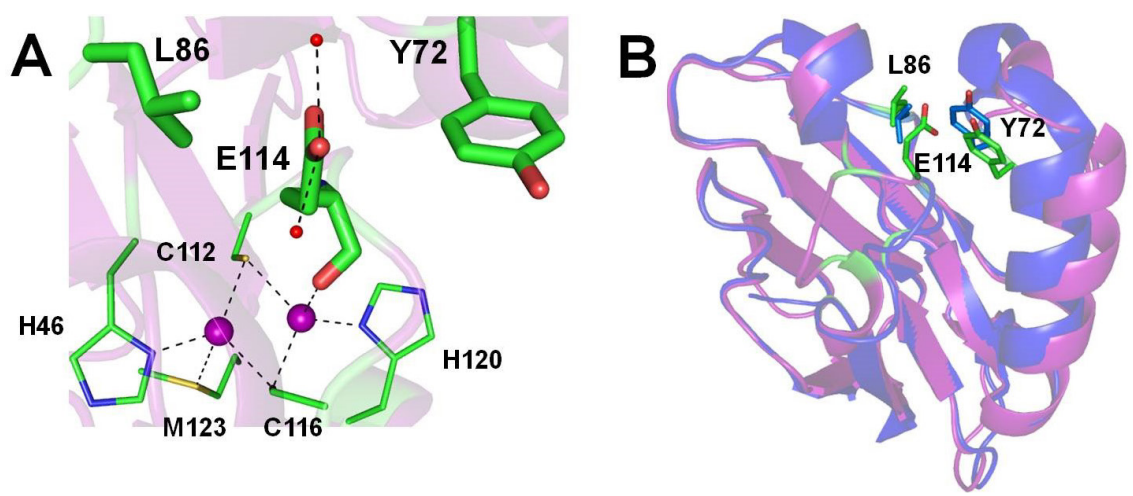


Figure 1. A. Orientation of the Glu114 side chain in Cu_AAz in between the two hydrophobic amino acids L86 and Y72, shown as sticks. Cu_A ligands are shown as lines, Cu atoms as purple spheres, water molecules that form hydrogen bonding interactions with the Glu114 side chain are shown as red spheres. Protein backbone is shown as cartoon. **B.** Cartoon representation of Cu_AAz (purple), and blue Cu Az (blue) showing how the placement of Glu114 side chain in Cu_AAz sterically pushes the two helices that house L86, and Y72, compared to the blue Cu Az. Figures were generated in PyMol.

of Cu(II)-substituted horse liver alcohol dehydrogenase (HLADH),⁶⁰⁻⁶² a Cu(II)-dithiolate complex was proposed as the identity of I_x. However, the exact ligand environment of I_x could not be established, as it was a short-lived intermediate present in a mixture with other species. The next step of the mechanism proposed the formation of a T1Cu complex from oxidation of the reduced Cu(I) product of I_x. The T1Cu complex was finally converted to the valence-delocalized Cu_A site via incorporation of *in situ* reduced Cu(I).

While the above results are valuable, they do not fully clarify the mechanism of the Cu_A formation. A critical missing piece of this mechanistic puzzle is the identity of the I_x intermediate. To identify this I_x , we examine the X-ray structure of Cu_AAz , which reveals that the side chain of Glu114, whose backbone carbonyl is very close to one of the Cu ions (2.2 Å), is positioned in between two hydrophobic amino acids, Leu86 and Tyr72 (**Fig. 1A**). ⁶³ We thus hypothesize that the Glu114 side chain is likely more solvent exposed in the apo form due to the negative charge on the Glu carboxylate at neutral

pH. In the holo form, the coordination of the backbone carbonyl group of Glu114 to one of the copper ions likely requires a specific orientation of the Glu114 side chain in between the two hydrophobic amino acids. As a result of this steric effect, the helices housing these two amino acids are pushed away from each other (**Fig. 1B**, purple). Interestingly, no such steric repulsion of the helices in blue T1Cu Az is observed (**Fig. 1B**, blue). In contrast, the corresponding Glu side chain, found in the majority (80%) of native CcOs is oriented towards the membrane interior, where it is coordinated to a Mg(II) ion.¹⁴

Herein, we investigate the effect of the Glu114 side chain on the sterics of the Cu binding loop and on the Cu_A assembly, by systematic substitution of this side chain with other side chains such as Gly (lacking a side chain), Ala (having a smaller, more hydrophobic methyl group), Leu (same chain length but more hydrophobic), and Gln (same chain length, but with no charge). Thus, the Gly, Ala, and Leu mutations would allow us to test the effect of increasing side chain bulk, while the Leu and Gln mutations should address the role of side chain polarity on the mechanism of the Cu_A formation. The specific issues we try to address in this report are: a) whether these mutations have any effect on the overall mechanism of Cu_A formation, in particular the rate of the $T2Cu \rightarrow I_X$ step of the mechanism, as this step was proposed to involve a conformational change in the metal binding loop, and b) whether these mutations affect the formation and decay kinetics of these intermediates. Of particular interest was to obtain the I_X in higher purity compared to the original Cu_AAz and determine its identity.

Materials and Methods

Protein **Expression** and Purification. Plasmids of the Cu_AAz variants Glu114Gly/Ala/Leu/Gln containing a periplasmic leader sequence from *Pseudomonas* aeruginosa were cloned into pET-9a vector and expressed in E.coli BL21*(DE3) (Invitrogen) competent cells. Expression and purification was done as described previously, 38, 44, 58, 59 with some modifications. Bacterial cultures were grown in 2XYT media at 25°C until an OD of ~0.6-1.0 was reached. Protein expression was induced with Isopropyl β-D-1-thiogalactopyranoside (IPTG) (~200mg/2L) and allowed to grow for 4 hours. Cells were harvested and re-suspended in 20% sucrose, 1 mM Ethylenediaminetetraacetic acid (EDTA), 30 mM 2-Amino-2-hydroxymethyl-propane-1,3-diol (Tris).HCl solution. After centrifugation the periplasmic membranes were lysed by osmotic shock solution containing 4 mM NaCl and 1 mM Dithiothreitol (DTT). Following centrifugation, the supernatant was treated with 500 mM NaOAc pH 4.1 to precipitate the impurities. The solution was centrifuged one final time and the supernatant was applied to SP Sepharose cation exchange column (GE Healthcare) pre-equilibrated with 50 mM NH₄OAc pH 4.1, and the protein was eluted using a shallow gradient of 50 mM NH₄OAc pH 6.35. The fractions containing the apo protein were pooled, pH adjusted to 6.3 and further purified by HiTrap Q-Sepharose anion exchange column (GE Healthcare). The colorless apo protein was then concentrated to ~10 mL and further subjected to a size exclusion column (Sephacryl S100, GE Healthcare) to separate misfolded protein. 50 mM NH₄OAc pH 6.35 was used as the elution buffer. The purity and the identity of the properly folded apo protein were verified by electrospray ionization mass spectrometry. Aliquots of apo proteins were flash frozen and stored at -80° C until further use. Whenever required, the apo protein was thawed, exchanged into Universal Buffer (UB) containing 40 mM 2-(*N*-morpholino)ethanesulfonic acid (MES), 3-(N-morpholino)propanesulfonic acid (MOPS), Tris, and, N-cyclohexyl-2-hydroxyl-3-aminopropanesulfonic acid (CAPS), 50 mM NaOAc, and 100 mM NaNO₃ at the appropriate pH using Sephadex G-25 desalting columns and concentrated to the required concentration using Amicon Ultra filtration membranes (Millipore). Protein concentrations were determined using $\epsilon_{280} = 8440 \text{ M}^{-1}\text{cm}^{-1}$.

Stopped flow UV-vis Absorption Spectroscopy. Stopped flow UV-Vis absorbance data were collected on an Applied Photophysics Ltd. (Leatherhead, U.K.) SX18.MV stopped flow spectrophotometer equipped with a 256 element photodiode array detector. Equal volumes of 0.5 mM apo protein in UB pH 7 (UB 7) and 0.2 mM CuSO₄ solutions (1.0 : 0.4 eq. protein : CuSO₄ ratio) were mixed by two syringes and spectra were collected over 1000 s on logarithmic scale containing 200 data points with 1 ms sampling time. The final concentrations of protein and CuSO₄ were 0.25 mM and 0.1 mM, respectively. A water bath connected to the instrument was used to maintain the temperature at 15°C. For anaerobic stopped-flow experiments the protein and the buffer were degassed on a Schlenk line by three freeze-pump-thaw cycles. Prior to mixing, the stopped-flow instrument was washed with degassed buffer. Similarly, for O₂-rich experiments, the buffer was made O₂-saturated by purging with O₂ for ~15 minutes prior to the experiments. Raw data were subjected to global analysis using SpecFit/32 (Spectrum Software Associates, Inc.).

Global Fit Analysis of the Stopped flow Data. The raw stopped-flow data were processed using SpecFit/32 in order to deconvolute the complex spectral features and multiple kinetic processes. The data analysis is based on Single Value Decomposition (SVD) and non-linear least square fits of the experimental data in an iterative process. During the fitting process a set of kinetic models that seem most consistent with the experimental data were input into the software and fit globally. Using the information from the initial fitting process, the kinetic models were modified accordingly until satisfactory fit results were obtained based on statistics and kinetic parameters.

Kinetic UV-vis Absorption Spectroscopy. Kinetic UV-vis absorption data of samples containing 0.25 mM apo protein in UB 7 and 0.1 mM CuSO₄ were collected with

constant stirring at 10°C on an Agilent 8453 photodiode array spectrophotometer connected with a water bath cooling system. A lower temperature (10°C) was chosen in the kinetic UV-vis absorption experiment than that (15°C) in the stopped-flow UV-Vis absorption experiment, because of concerns of potential stability issue of the proteins at much longer time scale in the kinetic UV-vis absorption experiment than that in the stopped-flow experiment. Because of this temperature difference, the kinetic rate constants (see Table 1) were obtained only from the stopped-flow data. For these experiments, 1000 µL of 0.5 mM apo protein in UB 7 was taken on a 1cm x 1cm cuvette with stirring and the instrument was set to collect data for 3600 s with scan time of 0.5 s incremented by 5% after 30 s to reduce the number of data points. After collecting a few spectra, 1000 μL of 0.2 mM CuSO₄ was added to the apo protein and the cap of the cuvette was sealed with parafilm. The final concentrations of protein and CuSO₄ were 0.25 mM and 0.1 mM. After 3600 s, another experiment was started to continue for additional 10-24 hours using a longer scan time of 600 s as the later kinetic processes were slow. In other instances, similar experiments were performed with solutions containing equal volume of 3 mM apo protein in UB 7 and 1.2 mM CuSO₄, amounting to a final concentration of 1.5 mM apo protein and 0.6 mM CuSO₄. These experiments were performed at the concentrations similar to those of target EPR experiments, so as to determine the time points at which different intermediates formed with maximum population in order to characterize them by EPR. Due to fast formation and decay of the red T2 Cu intermediate (~100 ms), we focused on characterizing the later intermediates, in particular Ix, as this intermediate was not thoroughly characterized previously. From inspection of the UV-vis absorbance data from these experiments, Ix formed with maximum population at ~50-60 s.

Electron Paramagnetic Resonance Spectroscopy. EPR data were collected using an X-band Varian E-122 spectrometer at the Illinois EPR Research Center (IERC) at 30 K using liquid He and an Air Products Helitran cryostat. Magnetic fields were calibrated with a Varian NMR Gaussmeter while the microwave frequencies were measured with an EIP frequency counter. Based on the results of the kinetic UV-vis experiments, EPR samples were flash frozen in liquid N2 with 22% glycerol as glassing agent at a broad range of time points after CuSO₄ addition. The time points were chosen so as to obtain as much information as possible about the discrete kinetic processes and the species present therein at that time point. The earliest time points were determined to capture the I_x in each mutant. The earliest time point (50s-60s) samples were prepared by quick mixing of equal volumes of 3 mM apo protein in UB 7 and 1.2 mM CuSO₄ premixed with glycerol to give a final concentration of 1.5 mM protein, 0.6 mM CuSO₄. For longer time point samples (5 min - 24 hours), a pool of apo protein and CuSO₄ was mixed together, stirred at 10°C while aliquots from the mixture were frozen at desired time points to monitor either the decay of I_x, or formation of T1Cu intermediate or the formation of the final CuA form, after adding glycerol to a final concentration of 22%. All samples for longer time points had the same starting concentrations of apo protein and CuSO4 as

the samples frozen at the earliest time points, to be consistent. Pure holo Cu_A forms of each variant were prepared by adding a solution of premixed 0.8 eq. Cu(I) and 0.8 eq. CuSO₄ to the apo protein in UB 7. Sub-stoichiometric Cu was added to ensure no present in solution. Cu(I) was added in the form tetrakis(acetonitrile)copper(I)hexafluorophosphate. Experimental EPR data were simulated using SIMPOW6.64 All the spectra were fit simultaneously to obtain relative populations and EPR parameters of various species so as to minimize the total rms difference between experimental and simulated spectra. For spin quantification, CuSO₄ standards were prepared at concentrations ranging from 2 – 0.0625 mM. EPR data for the standards and the protein samples were collected at a constant temperature and power of 30K, and 0.2 mW, respectively. Instrument gain was normalized across all samples. Standard curve was obtained by plotting the double integration area as a function of CuSO₄ concentration. Cu(II) concentration in protein samples were calculated from the standard curve.

X-ray Absorption Spectroscopy. The Extended X-ray Absorption Fine Structure (EXAFS) spectra were collected at beam line X3B, National Synchrotron Light Source with a sagittally focused Si (111) crystal monochromator. Samples were cooled to 10K before scanning and kept cold during data collection. Kα fluorescence was collected by a Canberra 31-element Ge detector. A Cu foil was used as reference to calibrate energy. A 6μm Ni filter was placed before detector to reduce elastic scattering. Six scans of each sample were collected. These samples were prepared using similar procedure as described in the EPR section. Samples contained 5.2 - 5.8 mM apo protein in UB 7, 2.08-2.32 mM CuSO₄ [1:0.4 ratio of apo protein to Cu(II)] to a final concentration and flash frozen in liquid N₂ at various time points (50 - 10 hours) after adding 20% ethylene glycol as the glassing agent. For earliest time points (50s - 60s) ethylene glycol and CuSO₄ were premixed prior to adding to the apo protein. Data reduction and background subtraction were performed with EXAFSPAK⁶⁵ and data was fitted with EXCURVE $9.2.^{66}$

Results and Discussions

Kinetics of Cua Reconstitution in Glu114Gly/Ala/Leu/GlnCuaAz. The kinetic processes of Cua reconstitution in Glu114Gly/Ala/Leu/GlnCuaAz were monitored by stopped flow and standard UV-vis absorption spectroscopy in the presence of subequivalent amounts of CuSO4. Addition of 0.4 eq. CuSO4 to 0.25 mM Glu114GlyCuaAz led to the formation, within 100 ms, of a species displaying an intense peak at 390 nm and a weak absorption peak at \sim 625 nm (**Fig. 2A**). The intense absorption centered at 390 nm is characteristic of the $S_{Cys(\sigma)} \rightarrow Cu(II)$ charge transfer (CT) transition of a red T2Cu species. Over the next 50s, an intermediate species formed exhibiting two

intense S_{Cys}→Cu CT transitions at 413 nm (sharp) and 616 nm (broad), plus a broad peak at 762 nm. These features are similar to the previously reported intermediate X (I_x).⁵⁹ The 413 nm peak formed faster than the 616 nm peak over the next 14 minutes, and also decayed faster. At the end of 14 minutes, the 413 nm peak red shifted to 420 nm, and the 616 nm peak blue shifted to ~610 nm, indicating the formation of blue T1Cu species. Over the next 5 hours, as monitored using separate kinetic UV-vis experiments (see materials and methods for details) the intense absorption bands at 420 and 610 nm attributable to T1Cu decayed, and the peaks for Cu_A at 478 nm, 534 nm, and 795 nm (**Fig. 2A**, inset) fully developed. Unlike other variants (*vide infra*), the kinetic processes of Glu114GlyCu_AAz did not display any isosbestic point at any time point. Analysis of the stopped flow data (1000 s) was performed using a kinetic model involving the formation of the early red T2Cu intermediate followed by the formation of I_x and the T1Cu (**Fig. S1, Table 1**).

Next we investigated the kinetics of Cu incorporation into the Glu114AlaCu_AAz variant. Similar to Glu114GlyCu_AAz, an early red T2Cu intermediate formed within 134 ms with an absorption band occurring at ~362 nm (**Fig. 2B**). A new intermediate species, corresponding to I_x, formed within the next 50 s, with intense peaks at 412 nm and 624 nm, and a broad feature at ~774 nm. This process was accompanied by an isosbestic point occurring at 390 nm. The intensity of the 412 nm peak was higher than that of the 624 nm peak. A small amount of Cu_A was also present. In the next ~900 s, the 412 nm peak decreased in intensity and red shifted to 426 nm, while the 624 nm peak blue shifted to 616 nm, with a concomitant increase in intensity. The new features are attributed to a blue T1Cu species that developed with isosbestic conversion from I_x. The 426 and 616 nm peaks of the T1Cu intermediate decayed over the next 10 hours, while absorptions in the regions typical of Cu_A increased, with isosbestic points occurring at 460 nm, and 556 nm (**Fig. 2B**, inset). The kinetic processes within the first 1000 s were modeled (**Fig. S1, Table 1**) similar to that of Glu114GlyCu_AAz.

For Glu114LeuCu_AAz, a red T2Cu intermediate with an intense absorption peak appearing at ~360 nm was also formed within 100 ms of mixing, (**Fig. 2C**), which decayed to I_x within 60 s with isosbestic point at 387 nm. The I_x displayed two intense absorption peaks at 413 nm, 470 nm, and a broad feature at ~793 nm. The intensity of the 413 nm peak was higher than that of the 470 nm peak. The I_x started to decay after 85 s, and was converted to a blue T1Cu intermediate with peaks occurring at 467 nm, 614 nm and a weak band at 793 nm and isosbestic points at 560 nm, and 680 nm. The T1Cu was fully formed within 40 min and started to decay to Cu_A with an isosbestic point at 560 nm over 10 hours (**Fig. 2C**, inset). The stopped flow data were modeled in the same way as other variants (**Fig. S1, Table 1**).

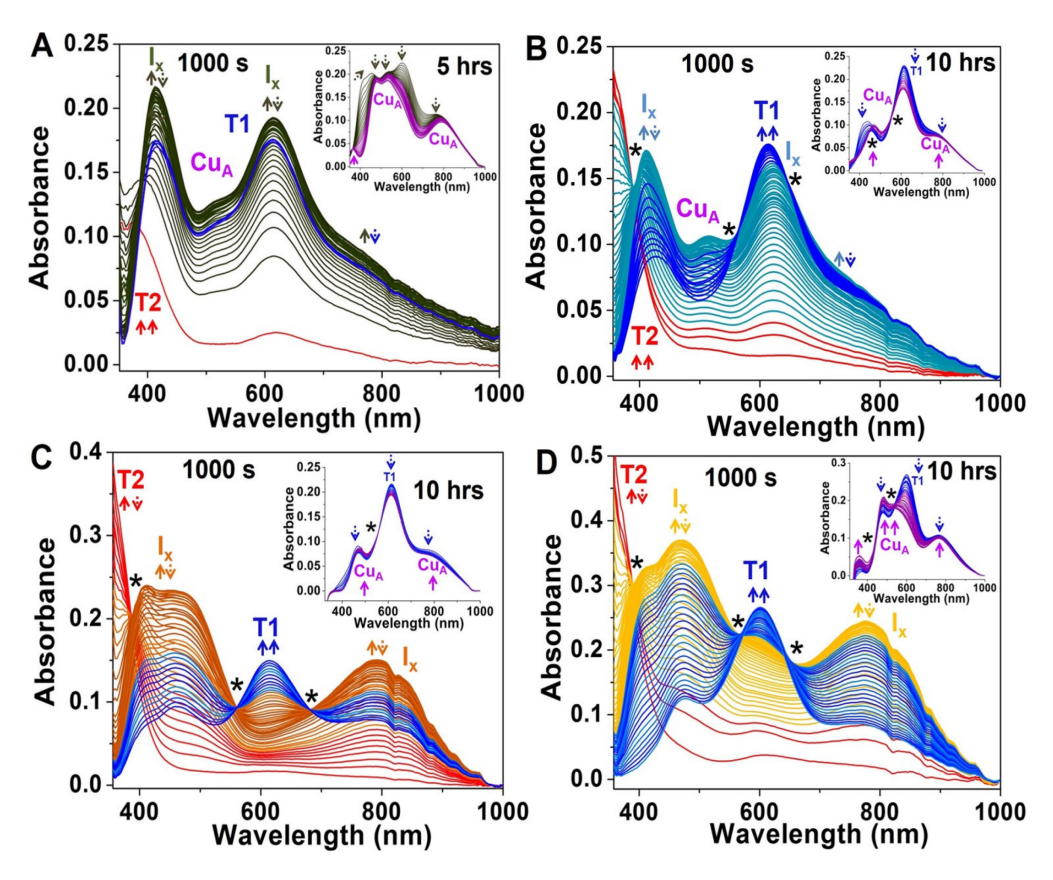


Figure 2. Stopped-flow spectra obtained after mixing 0.5 mM apo Glu114GlyCu_AAz (**A**), Glu114AlaCu_AAz (**B**), Glu114LeuCu_AAz (**C**), and Glu114GlnCu_AAz (**D**) in UB 7 buffer, with 0.2 mM CuSO₄. Insets show separate kinetic UV-vis experiments under the same condition, monitored for longer time. Isosbestic points are shown as asterisks (*). Unique UV-vis signatures for individual I_x (I_{x1} , and I_{x2}) as seen by EPR (*vide infra*) cannot be deconvoluted due to spectral overlap and are labeled as I_x . Up and down arrows indicate the formation and decay of various species.

Finally, in Glu114GlnCu_AAz, a red T2Cu intermediate displaying an intense peak at ~385 nm was observed within 100 ms of mixing (**Fig. 2D**). Within 50 s the I_x formed displaying two intense absorption bands at 409 nm, 470 nm, and a broad peak at ~790 nm with an isosbestic point at 390 nm. The 409 nm peak is slightly higher in intensity than the 470 nm peak. The I_x decayed to a blue T1Cu intermediate with isosbestic points at 572 nm and 653 nm. The T1Cu intermediate having peaks at 467 nm, 601 nm, and ~790 nm fully developed within 20 min. After 30 min from mixing, Cu_A started to form having a weak peak at ~351 nm, two intense peaks at 479 nm, 541 nm, and a broad feature at ~760 nm, formed with isosbestic points at 434 nm, and 531 nm. The full Cu_A formation was observed within 10 hours (**Fig. 2D**, inset). The kinetic processes in the first 1000 s were modeled as others (**Fig. S1, Table 1**).

Table 1. Kinetic models used to fit the stopped-flow data shown in **Fig. 2**. Rate constants obtained from global analysis using Specfit are shown.

Cu _A Variant	Kinetic Model	Rate Constants
Glu114GlyCu _A Az		$k_1 = 11.28 \pm 0.35 \text{ s}^{-1}$
		$k_2 = 1.95 \pm 0.03 \text{ s}^{-1}$
		$k_3 = (0.78 \pm 0.04) \times 10^{-3} \text{ s}^{-1}$
Glu114AlaCu _A Az	CuSO₄ → T2 Cu	$k_1 = 13.52 \pm 0.52 \text{ s}^{-1}$
	T2 Cu \rightarrow I _x	$k_2 = 0.46 \pm 0.01 \text{ s}^{-1}$
	I _x → T1 Cu	$k_3 = (1.75 \pm 0.05) \times 10^{-3} \text{ s}^{-1}$
Glu114LeuCu _A Az		$k_1 = 13.12 \pm 0.98 \text{ s}^{-1}$
		$k_2 = 0.34 \pm 0.01 \text{ s}^{-1}$
		$k_3 = (1.31 \pm 0.05) \times 10^{-3} \text{ s}^{-1}$
Glu114GlnCu _A Az		$k_1 = 9.36 \pm 0.66 \text{ s}^{-1}$
		$k_2 = 0.31 \pm 0.01 \text{ s}^{-1}$
		$k_3 = (2.37 \pm 0.06) \times 10^{-3} \text{ s}^{-1}$

Since no external reductant was added and the formation of the mixed valence Cu_A site requires Cu(I), the reducing equivalents must be supplied by the active site cysteines. To investigate the effect of oxygen on the overall kinetic processes, we performed stopped-flow experiments under O_2 -free and O_2 -rich conditions. The results showed that, in the absence of O_2 , no T1Cu intermediate was formed in any of the mutants, whereas under O_2 -rich condition, the rate of T1Cu formation from I_x was faster compared to normal atmospheric O_2 levels (**Fig. S2**, **Table S1**). These observations suggest a role of O_2 in the formation of the T1Cu species. The absorption at ~625 nm for I_x of $G_1 = 14 G_1 = 12 G_2 = 12 G_$

Effect of Glu114 Substitutions on the Rates of Formation and the Characteristics of the Intermediates. It has been previously proposed that the formation of the initial capture complex for Cu ion involves Cys116 as the Cu ligand close to the exterior of the protein.⁵⁹ Our results indicate that the initial rates of formation of the red T2Cu capture complex are quite similar in all the four variants (**Table 1**, **Fig. 3A**), suggesting that substitution of the Glu114 side chain has minimal effect on the formation of the capture complex. However, the rate of the formation of I_x from the red T2Cu complex is fastest in Glu114GlyCu_AAz (**Fig. 3B, Table 1**) among the four variants. In the previous study,⁵⁹

the formation of I_x from the T2Cu capture complex was proposed to involve a conformational change of the Cu_A loop, where the Cu-bound Cys116 reoriented from the protein exterior to the interior. Our results herein support this hypothesis, as the conformational change of the Cu_A loop required for the formation of I_x would be most favorable in Glu114GlyCu_AAz, because Gly has the least steric side chain and most flexible backbone conformation in the Ramachandran plot.⁶⁷ The presence of longer side chain groups in Ala, Leu, Gln or Glu would accordingly disfavor such a

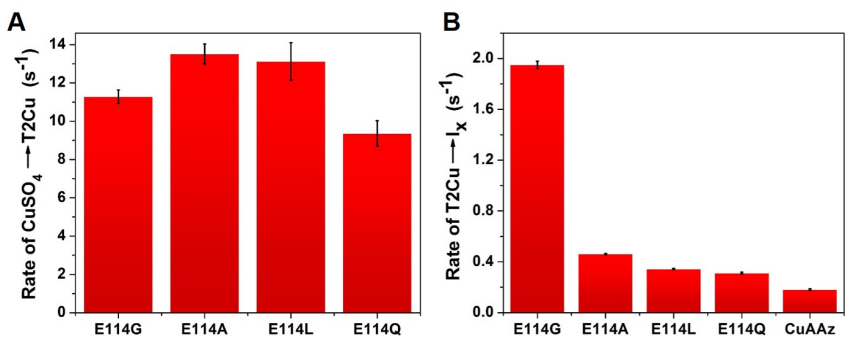


Figure 3. A) Rates of $CuSO_4 \rightarrow T2Cu$, and **B)** $T2Cu \rightarrow I_x$ conversion of Cu_A variants obtained from the Stopped-flow data. Rates in **A)** are similar in all variants. In **B)** highest rate is observed for $Glu114GlyCu_AAz$ which supports the hypothesis that the $T2Cu \rightarrow I_x$ conversion involves a conformation change of the Cu_A ligand loop as Gly has the most flexible backbone conformation, and thus favors such conformation change compared to the other amino acid side chains.

conformational change, owing to steric encumbrance from these side chains and less backbone flexibility. Taken together, these results suggest that backbone flexibility is an important factor in determining the rates of $T2Cu \rightarrow I_x$ formation. related studv involving *Tt* Cu_A the presence of а hydrophobic patch

involving Leu155 in the metal binding loop was shown to be important in facilitating ET between cytochrome c_{552} and the Tt Cu_A.⁶⁸

The kinetic data further suggest that the nature of the Glu114 side chain influences the timescales on which these intermediates are formed, the wavelengths of the absorption peaks, and how cleanly one intermediate is converted to another. For example, in Glu114GlyCuAAz, no isosbestic point was observed during any of the kinetic processes, whereas, in the other three variants, well-defined isosbestic points were observed for conversions between different species. The cleanest conversion from one intermediate to another was observed in Glu114LeuCuAAz, and Glu114GlnCuAAz, where minimal spectral overlap among different species was present. In contrast, a strong overlap between the Ix, and T1Cu intermediates was observed in the other two variants. Interestingly, the split peaks for the Ix at 410, and 470 nm were observed only in Glu114LeuCuAAz, and Glu114GlnCuAAz. Additionally, the relative intensities of these two peaks are reversed in Glu114LeuCuAAz, and Glu114GlnCuAAz, where the 410 nm peak is more intense in the former, whereas the 470 nm peak has higher intensity in the

latter variant. These observations, therefore, indicate that Glu114 side chain plays a role in dictating the characteristics of the intermediates.

EPR Studies of the I_x **species:** To further understand the nature of the intermediates, in particular, I_x , we collected X-band EPR data of two representative variants, the Glu114GlyCu_AAz that did not display kinetic isosbestic point and Glu114GlnCu_AAz that did. The EPR spectrum of Glu114GlyCu_AAz collected at 50s (the time point at which the I_x formed with maximum population) (**Fig. 4a**) was simulated as two mononuclear Cu(II) species in almost equal population (38% and 46%, respectively). From the simulations, the g_z and A_z values for the two I_x were extracted to be 2.152, $101x10^{-4}$ cm⁻¹, for I_{x1} , and 2.185, $90x10^{-4}$ cm⁻¹ (**Table 2**) for I_{x2} , respectively. While the Z-components of

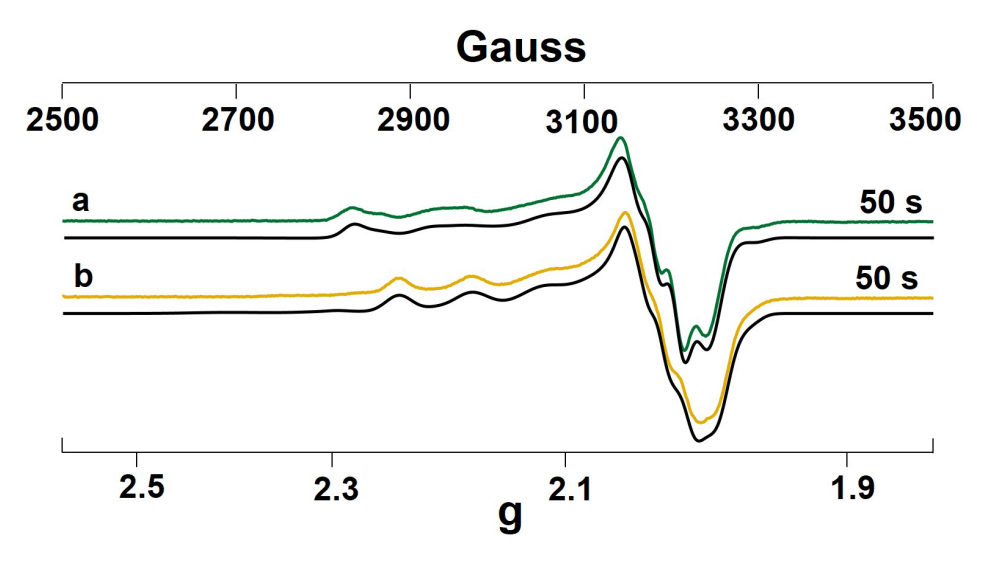


Figure 4. X-band EPR spectra of samples containing 1.5 mM Glu114GlyCu_AAz (\mathbf{a}), and Glu114GlnCu_AAz (\mathbf{b}), and 0.6 Mm CuSO₄, prepared at 50 s post-mixing. Experimental parameters: H = 9.053 GHz, T=30 K, Modulation = 4G, Microwave power = 0.2-0.5 mW. Simulated spectra are shown in black.

hyperfine couplings (A_z) are similar in both I_{x1} and I_{x2} that fall in between those of T1Cu and T2Cu complexes, their g_z values differ significantly from each other.^{10, 69} A smaller g_z value in I_{x1} suggests that the strength of the thiolate-Cu interaction is slightly stronger in I_{x1} in comparison to I_{x2} . Both the g_z and A_z for I_{x1} is similar to the Sco protein (g_z =2.150).⁴⁵ In addition, the A_z value is similar to the intermediate observed in Tt Cu_A (A_z = 109 x10⁻⁴ cm⁻¹).⁵⁶ In both of these systems, copper is present as a bis-thiolate Cu(Cys)₂His complex. By analogy, we assign the I_{x1} having a similar ligand environment to these two Cu(II) centers. The I_{x2} with a g_z of 2.185 is lower than most T1Cu sites (g_z ~2.190-2.300).¹⁰ The I_{x2} can be best assigned as having a slightly different ligand coordination/geometry around the metal site relative to that of I_{x1} .

For Glu114GlnCu_AAz, two mononuclear Cu(II) species were also observed at 50 s (time point at which the I_x formed with maximum population), but with unequal populations of 68% and 18%, respectively (**Fig. 4b**). The first species has a g_z of 2.151 and A_z of 82×10^{-4} cm⁻¹ (**Table 2**), which is indicative of a species with a strong thiolate-Cu interaction and can be assigned as I_{x1} with Cu(Cys)₂His ligation, using a similar analogy to the I_{x1} of Glu114GlyCu_AAz. The second species, I_{x2} , present in 18% population, has a g_z of 2.249 and A_z of 133×10^{-4} cm⁻¹. Although both the g_z and A_z values are higher than the I_{x2} of Glu114GlyCu_AAz, these parameters are similar to the Cu(Cys)₂(His)L (L=pyrazole, NADH) complex of HLADH (g_z =2.200, A_z =115 x10⁻⁴ cm⁻¹). $^{60-62}$ Based on this similarity, we assign the I_{x2} of Glu114GlnCu_AAz as having a similar Cu(Cys)₂(His)L (L=weak axial ligand) ligation/geometry.

Table 2. EPR parameters extracted from simulation of the early time points EPR spectra shown in **Fig. 4**.

On Variant	Developing 2								
Cu _A Variant	Parameters	I _{x1}	I _{x2}	Time	$\begin{tabular}{lll} \hline Populations^a \\ \hline Time & I_{x1} & I_{x2} \\ \hline \end{tabular}$				
Glu114GlyCu₄Az	g_x g_y g_z $ A_x x10^{-4} \text{ cm}^{-1}$ $ A_y x10^{-4} \text{ cm}^{-1}$ $ A_z x10^{-4} \text{ cm}^{-1}$	2.034 2.044 2.152 10 6 101	2.027 2.020 2.185 23 22 90	50 s	38%	46%			
Glu114GlnCu _A Az	g_x g_y g_z $ A_x \times 10^{-4} \text{ cm}^{-1}$ $ A_y \times 10^{-4} \text{ cm}^{-1}$ $ A_z \times 10^{-4} \text{ cm}^{-1}$	2.011 2.035 2.151 20 14 82	1.991 2.092 2.249 8 41 133	50 s	68%	18%			
CuaAz ⁵⁹	g_x g_y g_z $ A_x $ x10 ⁻⁴ cm ⁻¹ $ A_y $ x10 ⁻⁴ cm ⁻¹		2.007 2.056 2.234 9 0.3 115						
<i>Tt</i> Cu _A ⁵⁶	g_x g_y g_z $ A_x x10^{-4}$ cm ⁻¹ $ A_y x10^{-4}$ cm ⁻¹ $ A_z x10^{-4}$ cm ⁻¹	2.013 2.052 2.134 16 16 109							

^aOnly I_x present in the earliest time points are shown. See Table S2 for time-dependent populations of various species and their EPR parameters. Based on higher g_z of Cu_AAz, the I_x can be categorized as I_{x2s} in the variants.

These EPR data also suggest that a small amount of Cu_A is formed along with the I_X (**Table S2**). Subsequently, the I_X decayed and more T1Cu and Cu_A formed (see the SI). The pure Cu_A forms of each variant show the expected well-resolved seven-line hyperfine pattern, as well as the characteristic EPR parameters (**Fig. S3 Table S3**).

X-ray Absorption Spectroscopy: To probe the ligand and coordination environment of the I_x , Cu k edge X-ray absorption spectroscopy was used. The EXAFS data for the I_x of Glu114GlyCuAAz was best simulated as 2 Cu-S_{Cys} ligands at 2.17 Å, and 1 Cu-N_{His} ligand at 1.97 Å (**Fig. 5A**, **Table 3**). For Glu114GlnCuAAz, the EXAFS data (**Fig. 5B**) for the I_x was best simulated as 1 Cu-N_{His} at 1.93 Å, and 2 Cu-S_{Cys} at 2.20 Å (**Table 3**). According to EPR simulation, two I_x species are present at this time point with slightly different ligand geometry (*vide supra*). However, as EXAFS measures average Cu-ligand distances, the individual Cu(II) species cannot be deconvoluted from the EXAFS data.

In the I_x of these variants the $Cu(Cys)_2His$ ligand coordination is similar to what was observed for the green intermediate in Tt Cu_A as well as for the Sco protein. ^{45, 56, 59} The EXAFS spectra and data analysis of the holo Cu_A samples of the Glu114XCu_AAz variants are consistent with other reported Cu_A systems (**Fig. S4**, **Table S4**). ⁵⁶

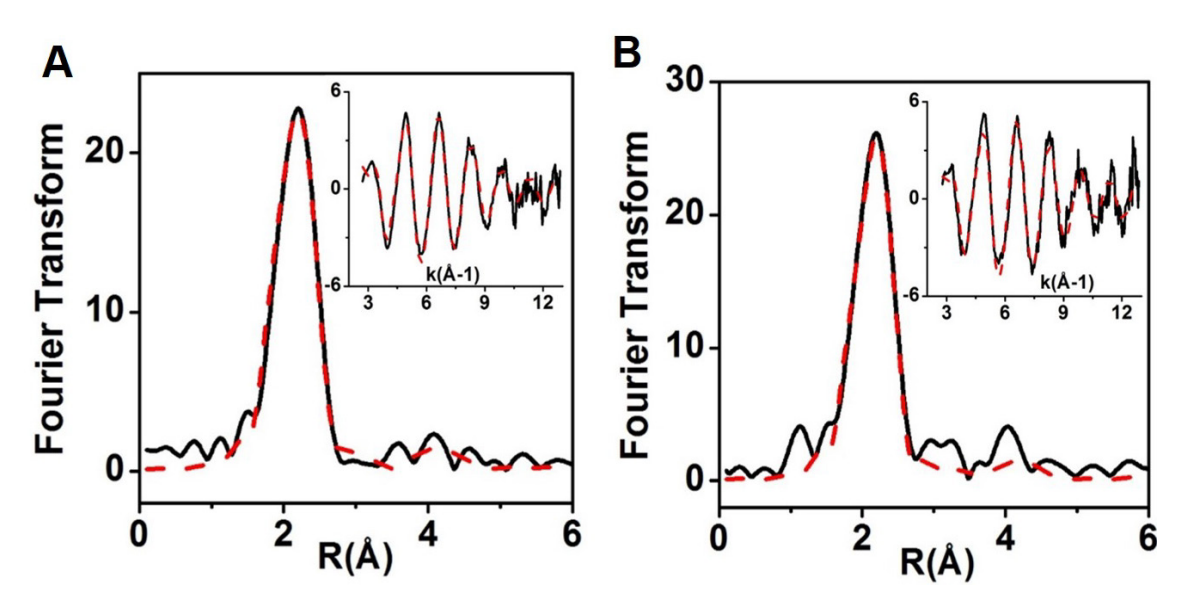


Fig. 5. Fourier transform and EXAFS (inset) data of 50s samples of Glu114GlyCu_AAz ($\bf A$), and Glu114GlnCu_AAz ($\bf B$). Experimental data are shown as solid black lines and simulation are shown as dashed red lines. Parameters used to fit data are shown in Table 3.

Table 3. Parameters extracted from fitting of the EXAFS data of I_x .

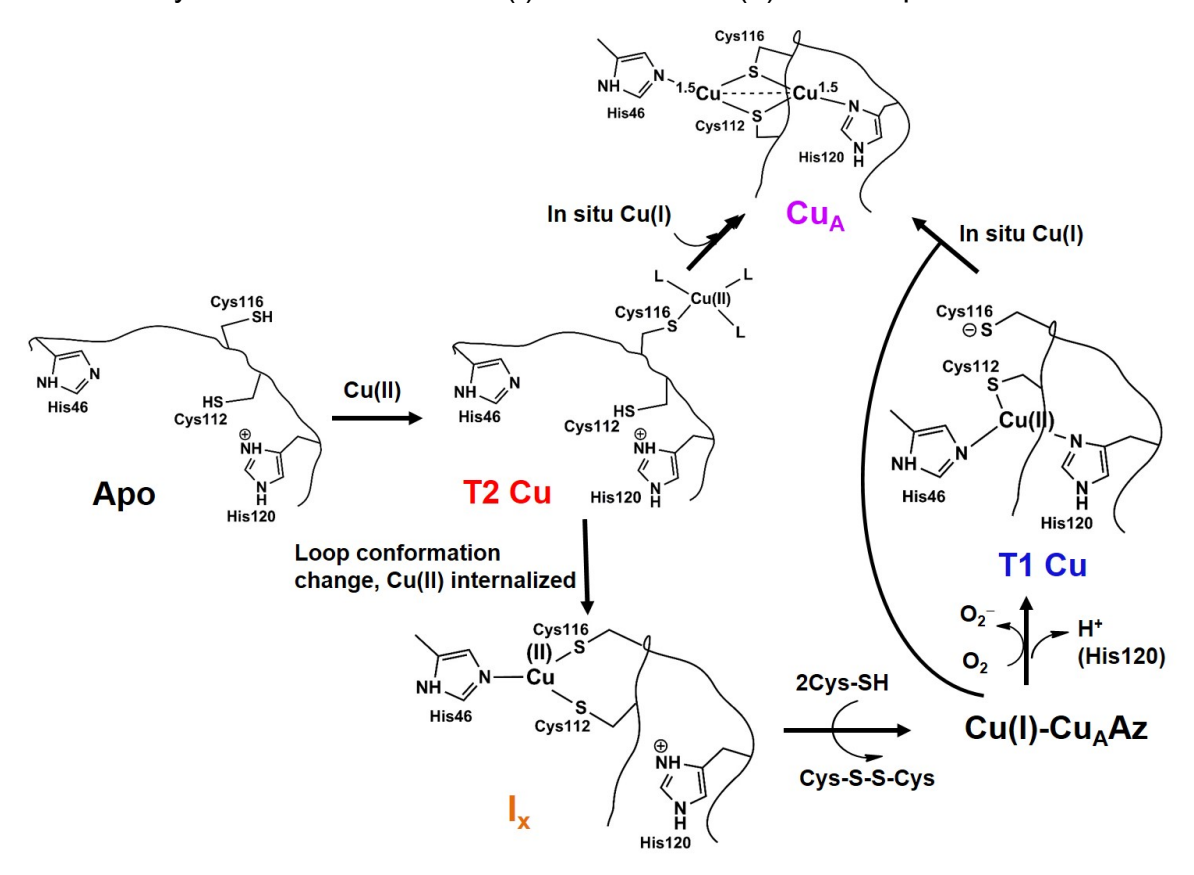
Sample/Fit	F	Cu-S (Cys)		Cu-N (His)			Cu-Cu ^a			_	
		N	R(Å)	DW(Ų)	N	R(Ų)	DW(Å)	N	R(Å)	DW(Ų)	E₀
Glu114GlyCu _A Az	0.53	2	2.17	0.016	1	1.97	0.02	0.15	2.412	0.0035	-0.76
Glu114GlnCu₄Az	0.60	2	2.20	0.012	1	1.93	0.005	0.1	2.340	0.005	1.52

^aSmall amounts of the binuclear Cu_A forms present at the earliest time point samples.

Proposed Mechanism of Cu_A Formation: The combined UV-vis, EPR, and EXAFS data presented in this work has allowed us to propose a mechanism of Cu_A formation in these Cu_AAz variants (Scheme 1). Upon addition of sub-equivalent Cu(II) to the apo proteins, an initial red T2Cu capture complex is formed within ~100 ms. Previous results from Cu_AAz established that the T2Cu capture complex is formed close to the exterior of the protein with Cys116 as the only protein-derived ligand.^{44, 59} The next step of the mechanism is bifurcated (Scheme 1): conversion of T2Cu to I_x, and formation of a small population of Cu_A in a direct pathway from the T2Cu complex. Previously, it was hypothesized that T2Cu to I_x formation involved a conformation change of the Cu_A loop by which the capture complex is internalized from the protein exterior. Our results in this work show that T2Cu to I_x formation is fastest in Glu114GlyCu_AAz compared to the other mutants. As Gly has the most flexible backbone conformation, this observation, therefore, supports the hypothesis that indeed T2Cu to I_x formation is facilitated by swinging of the Cu_A loop, which brings the Cu to the protein interior.

In the next step the I_x decay and T1Cu complexes form within ~15 minutes. The formation of T1Cu complex is dependent on the presence of O_2 , as the T1Cu species does not form in the absence of O_2 (**Fig. S2**). Since, in all cases, the decay of I_x is accompanied by the formation of the T1Cu species in the presence of O_2 , it can be inferred that the T1Cu complex is a result of the oxidation of the decay product of I_x . EPR spin quantification shows that the I_x of Glu114GlyCuAAz decay with time (**Fig. S5**), indicating spin loss due to the formation of the EPR silent Cu(I) species. Therefore, the T1 Cu is a product of the oxidation of Cu(I) formed during the decay of I_x . At even longer time scale, the T1Cu complex decays and CuA start to form (**Fig. 2**, insets). Formation of the binuclear CuA from T1Cu complexes must be achieved by reaction of the T1Cu species with either free Cu(I) generated *in situ* or with Cu(I)-CuAAz.

The formation of a small population of Cu_A from T2Cu as observed here must be achieved by reaction of free Cu(I) with the Cu(II)-loaded protein. As no external



Scheme 1. Proposed mechanism of Cu_A formation in $Glu114XCu_AAz$ variants. Identity of the residues in the intermediates, and the protonation state of His120 have not been experimentally verified for the variants, and are proposed from what is known about Cu_AAz .

reductant was added, the Cu(I) must be generated *in situ* by the reduction of Cu(II) to Cu(I) by the active site cysteines of an apo Cu_A site. As the oxidation of cysteines to cystine is a $2e^-$ process, more than one Cu(II)-bound proteins must be interacting with each other to receive the reducing equivalents from the cysteine thiols. Alternatively, Cu(I) may also be generated by the reaction of free Cu(II) with the I_x , as suggested in the case of Tt Cu_A system. ⁵⁶ It is highly unlikely that nature only uses Cu(II) to metallate the Cu_A sites as it would be a significant waste of apo proteins to supply the reducing equivalents. Using both Cu(II) and Cu(I) would make the metallation process much more efficient as also shown in Tt Cu_A. ⁵⁶ The yield of holo Cu_A in the Glu114XCu_AAz variants significantly increased while using a mixture of Cu(II) and Cu(I) (**Table S3**).

Identity of Intermediate X (I_x): A major focus of this study is to determine the ligand and coordination environment of the I_x using the Glu114XCu_AAz variants. In the previous kinetic study of Cu_AAz, at the time when the I_x was formed with maximum population (~55% at ~30s), significant populations of other types of Cu species (Cu_A',

T1Cu) were present.⁵⁹ As a result, the identity of this species could not be experimentally determined. In contrast, the Ix in these CuA variants presented here can be obtained with a maximum of ~80-85% combined population, with only a minor percentage of CuA coexisting with the Ix. The electronic absorption data of the Glu114XCu_AAz variants indicate two sharp peaks in the 410-600 nm region and a broad feature at ~700-800 nm, similar to the pyrazole-substituted HLADH, which displays two peaks at ~400-500 nm, and a broad feature ~600-800 nm. 60-62 The EPR results indicate the presence of mononuclear T2Cu species with thiolate ligands. In all the variants, the EPR data suggest two mononuclear Cu complexes with minor differences in ligand coordination/geometry. Comparing the EPR parameters of the Ix1 to the green intermediate in Tt CuA and Cu(II)-Sco proteins (Table 2), the Ix1 intermediate observed in the Glu114GlyCuAAz, and Glu114GlnCuAAz variants can be best described as Cu(Cys)₂(His) complexes in trigonal geometry, while the I_{x2} can be best described as Cu(Cys)₂(His)L (L = weak axial ligand) complex in distorted tetrahedral geometry. The proposed ligands and geometries are consistent with EXAFS data, which can be modeled as 3-coordinate mononuclear Cu(Cys)₂His complex. Therefore, a combined UV-Vis, EPR, and EXAFS data indicate the presence of Cu-bisthiolato complexes with slightly different ligation/geometry as the identity of these intermediates (Fig. 6).

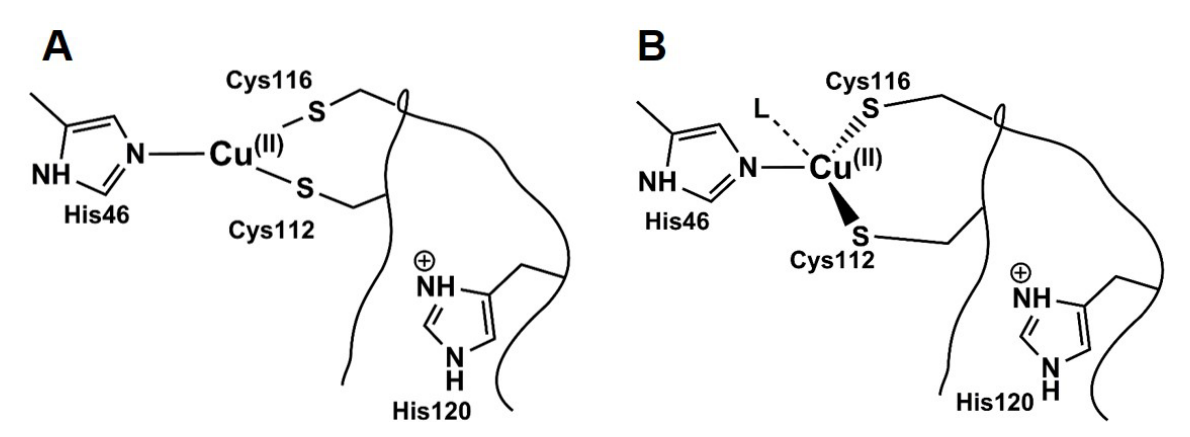


Fig. 6. Schematic representation of the proposed identity of different I_x in the Cu_A variants. Two mononuclear I_x with 3-coordinate $Cu(Cys)_2(His)$ ligation for $I_{x1s}(A)$, and as $Cu(Cys)_2(His)L$ (L= weak axial ligand) complex in distorted tetrahedral geometry for $I_{x2s}(B)$ are proposed. Absolute residue numbering has not been experimentally assigned.

Conclusions

We have investigated the influence of a key Cu_A ligand (Glu114) in Cu_A assembly as well as probed the nature of intermediates formed during *in vitro* reconstitution of the Cu_A center from Cu(II) ion and apo-forms of biosynthetic models in azurin (Cu_AAz). Our results show that the mechanism of Cu_A formation in variants of Glu114XCu_AAz (X=Gly,

Ala, Leu, Gln) proceeds via an initial formation of a red T2Cu center followed by another mononuclear intermediate X (Ix), then a T1Cu intermediate and finally the binuclear CuA center. The results showed that the Glu114 backbone flexibility is an important factor in determining the rates of T2Cu-)Ix formation, and suggest that CuA formation is facilitated by swinging of the ligand loop, which brings the external T2Cu complex to the protein interior. The kinetic data further suggest that the nature of the Glu114 side chain influences the timescales on which these intermediates are formed, the wavelengths of the absorption peaks, and how cleanly one intermediate is converted to another. This mechanistic investigation allowed us to find optimal conditions to obtain a high population of the I_x intermediate (80-85%), facilitating the use of UV-vis, EPR and EXAFS to elucidate the structure of Ix, which is best described as Cu(Cys)2(His) complex in trigonal geometry. While similar intermediates and mechanisms have been identified in native CuA, the exact structural features and pathways for the CuA formation are still not well understood. Our findings here of the mechanistic steps and the identification of key mononuclear intermediates during the assembly of the biosynthetic models of Cu_A in azurin and its variants have shed light into the mechanism of Cu_A formation.

Associated Content

Supporting Information:

Stopped flow data of Glu114XCuAAz variants under O₂-rich and anaerobic conditions, full EPR parameters of all intermediates, Specfit derived spectra of intermediates, EPR and EXAFS data of holo Glu114XCuAAz variants, and spin quantification of Glu114GlyCuAAz. This material is available free of charge via the Internet at http://pubs.acs.org.

Author Information

Corresponding authors:

*Emails: yi-lu@illinois.edu; blackbni@ohsu.edu

Present address:

§Center for Integrated Nanotechnologies, Los Alamos National Laboratory, Los Alamos, NM 87545, USA

[±] Department of Chemistry, Carnegie Mellon University, Pittsburgh, PA 15213, USA

- [⊥] Department of Chemistry, Reed College, Portland OR 97202, USA
- ⁺ University of Chinese Academy of Sciences, Beijing 100049, P. R. China

Funding

This work was supported by the U.S. National Science Foundation (CHE-1413328 to Y.L. and NSF Graduate Research Fellowship DGE-0925180 to K.N.C.) and U. S. National Institutes of Health (GM054803 to N.J.B. and 5T32-GM070421 to J.R.), and the Howard Hughes Medical Institute Exceptional Research Opportunities Program (to M.J.P.). The EXAFS data were collected at beamline X3B of the National Synchrotron Light Source (NSLS) at Brookhaven National Laboratory. Beamline X3B at NSLS is operated by the Case Center for Synchrotron Biosciences, supported by NIH NIBIB grant P30-EB-009998. NSLS is supported by the U.S. Department of Energy, Office of Science, Office of Basic Energy Sciences, under Contract No. DE-AC02-98CH10886. The contents of this publication are solely the responsibility of the authors and do not necessarily represent the official views of NIGMS or NIH

Notes

The authors declare no competing financial interest.

Acknowledgement

We wish to thank Dr. Arnab Mukherjee for helpful discussions.

References

- [1] Liu, J., Chakraborty, S., Hosseinzadeh, P., Yu, Y., Tian, S., Petrik, I., Bhagi, A., and Lu, Y. (2014) Metalloproteins Containing Cytochrome, Iron–Sulfur, or Copper Redox Centers, *Chem. Rev.* 114, 4366-4469.
- [2] Gray, H. B., Malmström, B. G., and Williams, R. J. P. (2000) Copper coordination in blue proteins, *J. Biol. Inorg. Chem.* 5, 551.
- [3] Vila, A. J., and Fernandez, C. O. (2001) Copper in Electron Transfer Proteins, In *Handbook on Metalloproteins* (Bertini, I., Sigel, A., and Sigel, H., Eds.), p 813, Marcel Dekker, New York, NY.
- [4] Wilson, T. D., Yu, Y., and Lu, Y. (2012) Understanding Copper-thiolate Containing Electron Transfer Centers by Incorporation of Unnatural Amino Acids and the CuA Center into the Type 1 Copper Protein Azurin, *Coord. Chem. Rev.* 257, 260-276.
- [5] Lu, Y., Chakraborty, S., Miner, K. D., Wilson, T. D., Mukherjee, A., Yu, Y., Liu, J., and Marshall, N. M. (2013) Metalloprotein Design, In *Comprehensive Inorganic Chemistry II* (Reedijk, J., and Poeppelmeier, K., Eds.), pp 565-593, Elsevier, Amsterdam.
- [6] Chakraborty, S., Hosseinzadeh, P., and Lu, Y. (2014) Metalloprotein Design and Engineering, In *Encyclopedia of Inorganic and Bioinorganic Chemistry* (Scott, R. A., Ed.), pp 1-51, John Wiley and Sons, Ltd., Chichester.
- [7] Farver, O., and Pecht, I. (2008) Elucidation of Electron-Transfer Pathways in Copper and Iron Proteins by Pulse Radiolysis Experiments, In *Prog. Inorg. Chem.*, pp 1-78, John Wiley & Sons, Inc.

- [8] Savelieff, M. G., and Lu, Y. (2010) Cu(A) centers and their biosynthetic models in azurin, *J. Biol. Inorg. Chem.* 15, 461-483.
- [9] Solomon, E. I., Heppner, D. E., Johnston, E. M., Ginsbach, J. W., Cirera, J., Qayyum, M., Kieber-Emmons, M. T., Kjaergaard, C. H., Hadt, R. G., and Tian, L. (2014) Copper active sites in biology, *Chem. Rev.* 114, 3659-3853.
- [10] Lu, Y. (2004) Electron transfer: Cupredoxins, In *Biocoordination Chemistry* (Que, J. L., and Tolman, W. B., Eds.), pp 91-122, Elsevier, Oxford, UK.
- [11] Solomon, E. I. (2006) Spectroscopic Methods in Bioinorganic Chemistry: Blue to Green to Red Copper Sites, *Inorg. Chem. 45*, 8012-8025.
- [12] Solomon, E. I., Xie, X., and Dey, A. (2008) Mixed valent sites in biological electron transfer, *Chem. Soc. Rev.* 37, 623-638.
- [13] Tsukihara, T., Aoyama, H., Yamashita, E., Tomizaki, T., Yamaguchi, H., Shinzawa-Itoh, K., Nakashima, R., Yaono, R., and Yoshikawa, S. (1995) Structures of metal sites of oxidized bovine heart cytochrome c oxidase at 2.8 A, *Science (Washington, DC, United States) 269*, 1069-1074.
- [14] Iwata, S., Ostermeier, C., Ludwig, B., and Michel, H. (1995) Structure at 2.8 A resolution of cytochrome c oxidase from Paracoccus denitrificans, *Nature 376*, 660-669.
- [15] Wikstrom, M. (2004) Cytochrome c oxidase: 25 years of the elusive proton pump, *Biochim. Biophys. Acta 1655*, 241-247.
- [16] Komorowski, L., Anemuller, S., and Schafer, G. (2001) First expression and characterization of a recombinant CuA-containing subunit II from an archaeal terminal oxidase complex, *J. Bioenerg. Biomembr.* 33, 27-34.
- [17] Komorowski, L., and Schafer, G. (2001) Sulfocyanin and subunit II, two copper proteins with novel features, provide new insight into the archaeal SoxM oxidase supercomplex, *FEBS Lett. 487*, 351-355.
- [18] Brown, K., Tegoni, M., Prudencio, M., Pereira, A. S., Besson, S., Moura, J. J., Moura, I., and Cambillau, C. (2000) A novel type of catalytic copper cluster in nitrous oxide reductase, *Nat. Struct. Biol.* 7, 191-195.
- [19] Zumft, W. G., and Kroneck, P. M. H. (2007) Respiratory transformation of nitrous oxide (N2O) to dinitrogen by Bacteria and Archaea, *Adv. Microb. Physiol.* 52, 107-227.
- [20] Suharti, Strampraad, M. J., Schröder, I., and de Vries, S. (2001) A Novel Copper A Containing Menaquinol NO Reductase from Bacillus azotoforman s, *Biochemistry 40*, 2632-2639.
- [21] Gamelin, D. R., Randall, D. W., Hay, M. T., Houser, R. P., Mulder, T. C., Canters, G. W., de, V. S., Tolman, W. B., Lu, Y., and Solomon, E. I. (1998) Spectroscopy of Mixed-Valence CuA-Type Centers: Ligand-Field Control of Ground-State Properties Related to Electron Transfer, J. Am. Chem. Soc. 120, 5246-5263.
- [22] Neese, F., Zumft, W. G., Antholine, W. E., and Kroneck, P. M. H. (1996) The Purple Mixed-Valence CuA Center in Nitrous-oxide Reductase: EPR of the Copper-63-, Copper-65-, and Both Copper-65- and [15N]Histidine-Enriched Enzyme and a Molecular Orbital Interpretation, J. Am. Chem. Soc. 118, 8692-8699.
- [23] Olsson, M. H., and Ryde, U. (2001) Geometry, reduction potential, and reorganization energy of the binuclear Cu(A) site, studied by density functional theory, *J. Am. Chem. Soc. 123*, 7866-7876.
- [24] Hulse, C. L., and Averill, B. A. (1990) Isolation of a high specific activity pink, monomeric nitrous oxide reductase from Achromobacter cycloclastes, *Biochem. Biophys. Res. Commun.* 166, 729-735.
- [25] Lappalainen, P., Aasa, R., Malmstrom, B. G., and Saraste, M. (1993) Soluble CuA-binding domain from the Paracoccus cytochrome c oxidase, *J. Biol. Chem. 268*, 26416-26421.

- [26] Slutter, C. E., Sanders, D., Wittung, P., Malmstrom, B. G., Aasa, R., Richards, J. H., Gray, H. B., and Fee, J. A. (1996) Water-soluble, recombinant CuA-domain of the cytochrome ba3 subunit II from Thermus thermophilus, *Biochemistry 35*, 3387-3395.
- [27] von Wachenfeldt, C., de Vries, S., and van der Oost, J. (1994) The CuA site of the caa3-type oxidase of Bacillus subtilis is a mixed-valence binuclear copper center, *FEBS Lett.* 340, 109-113.
- [28] Arciero, D. M., Hooper, A. B., and Rosenzweig, A. C. (2001) Crystal Structure of a Novel Red Copper Protein from Nitrosomonas europaea, *Biochemistry 40*, 5674-5681.
- [29] Arciero, D. M., Pierce, B. S., Hendrich, M. P., and Hooper, A. B. (2002) Nitrosocyanin, a red cupredoxin-like protein from Nitrosomonas europaea, *Biochemistry 41*, 1703-1709.
- [30] Ryden, L. G., and Hunt, L. T. (1993) Evolution of protein complexity: the blue copper-containing oxidases and related proteins, *J. Mol. Evol. 36*, 41-66.
- [31] Savelieff, M. G., Wilson, T. D., Elias, Y., Nilges, M. J., Garner, D. K., and Lu, Y. (2008) Experimental evidence for a link among cupredoxins: red, blue, and purple copper transformations in nitrous oxide reductase, *Proc. Natl. Acad. Sci. 105*, 7919-7924.
- [32] Farrar, J. A., Lappalainen, P., Zumft, W. G., Saraste, M., and Thomson, A. J. (1995) Spectroscopic and mutagenesis studies on the CuA centre from the cytochrome-c oxidase complex of Paracoccus denitrificans, *Eur. J. Biochem. 232*, 294-303.
- [33] Maneg, O., Ludwig, B., and Malatesta, F. (2003) Different Interaction Modes of Two Cytochrome-c Oxidase Soluble CuA Fragments with Their Substrates, *J. Biol. Chem. 278*, 46734-46740.
- [34] Paumann, M., Lubura, B., Regelsberger, G., Feichtinger, M., Koellensberger, G., Jakopitsch, C., Furtmueller, P. G., Peschek, G. A., and Obinger, C. (2004) Soluble CuA Domain of Cyanobacterial Cytochrome c Oxidase, *J. Biol. Chem. 279*, 10293-10303.
- [35] Slutter, C. E., Langen, R., Sanders, D., Lawrence, S. M., Wittung, P., Di Bilio, A. J., Hill, M. G., Fee, J. A., Richards, J. H., and et, a. (1996) Electron-transfer studies with the CuA domain of Thermus thermophilus cytochrome ba3, *Inorg. Chim. Acta 243*, 141-145.
- [36] Williams, P. A., Blackburn, N. J., Sanders, D., Bellamy, H., Stura, E. A., Fee, J. A., and McRee, D. E. (1999) The CuA domain of Thermus thermophilus ba3-type cytochrome c oxidase at 1.6 Å resolution, *Nat. Struct. Biol. 6*, 509-516.
- [37] Dennison, C., Vijgenboom, E., de Vries, S., van der Oost, J., and Canters, G. W. (1995) Introduction of a CuA site into the blue copper protein amicyanin from Thiobacillus versutus, *FEBS Lett. 365*, 92-94.
- [38] Hay, M., Richards, J. H., and Lu, Y. (1996) Construction and characterization of an azurin analog for the purple copper site in cytochrome c oxidase, *Proc. Natl. Acad. Sci. 93*, 461.
- [39] Jones, L. H., Liu, A., and Davidson, V. L. (2003) An Engineered CuA Amicyanin Capable of Intermolecular Electron Transfer Reactions, *J. Biol. Chem. 278*, 47269-47274.
- [40] van der Oost, J., Lappalainen, P., Musacchio, A., Warne, A., Lemieux, L., Rumbley, J., Gennis, R. B., Aasa, R., Pascher, T., and Malmstrom, B. G. (1992) Restoration of a lost metal-binding site: construction of two different copper sites into a subunit of the E. coli cytochrome o quinol oxidase complex, EMBO J. 11, 3209-3217.
- [41] Farver, O., Lu, Y., Ang, M. C., and Pecht, I. (1999) Enhanced rate of intramolecular electron transfer in an engineered purple CuA azurin, *Proc. Natl. Acad. Sci. 96*, 899-902.
- [42] Hay, M. T., Ang, M. C., Gamelin, D. R., Solomon, E. I., Antholine, W. E., Ralle, M., Blackburn, N. J., Massey, P. D., Wang, X., Kwon, A. H., and Lu, Y. (1998) Spectroscopic Characterization of an Engineered Purple CuA Center in Azurin, *Inorg. Chem. 37*, 191-198.
- [43] Hwang, H. J., Berry, S. M., Nilges, M. J., and Lu, Y. (2005) Axial Methionine Has Much Less Influence on Reduction Potentials in a CuA Center than in a Blue Copper Center, *J. Am. Chem. Soc.* 127, 7274-7275.

- [44] Hwang, H. J., Nagraj, N., and Lu, Y. (2006) Spectroscopic Characterizations of Bridging Cysteine Ligand Variants of an Engineered Cu2(SCys)2 CuA Azurin, *Inorg. Chem. 45*, 102-107.
- [45] Andruzzi, L., Nakano, M., Nilges, M. J., and Blackburn, N. J. (2005) Spectroscopic studies of metal binding and metal selectivity in Bacillus subtilis BSco, a homologue of the yeast mitochondrial protein Sco1p, *J. Am. Chem. Soc. 127*, 16548-16558.
- [46] Banci, L., Bertini, I., Cavallaro, G., and Ciofi Baffoni, S. (2011) Seeking the determinants of the elusive functions of Sco proteins, *FEBS J. 278*, 2244-2262.
- [47] Horng, Y.-C., Cobine, P. A., Maxfield, A. B., Carr, H. S., and Winge, D. R. (2004) Specific copper transfer from the Cox17 metallochaperone to both Sco1 and Cox11 in the assembly of yeast cytochrome C oxidase, *J. Biol. Chem. 279*, 35334-35340.
- [48] Nittis, T., George, G. N., and Winge, D. R. (2001) Yeast Sco1, a Protein Essential for Cytochrome cOxidase Function Is a Cu (I)-binding Protein, *J. Biol. Chem. 276*, 42520-42526.
- [49] Balatri, E., Banci, L., Bertini, I., Cantini, F., and Ciofi-Baffoni, S. (2003) Solution structure of Sco1: a thioredoxin-like protein involved in cytochrome c oxidase assembly, *Structure 11*, 1431-1443.
- [50] Banci, L., Bertini, I., Calderone, V., Ciofi-Baffoni, S., Mangani, S., Martinelli, M., Palumaa, P., and Wang, S. (2006) A hint for the function of human Sco1 from different structures, *Proc. Natl. Acad. Sci.* 103, 8595-8600.
- [51] Horng, Y.-C., Leary, S. C., Cobine, P. A., Young, F. B., George, G. N., Shoubridge, E. A., and Winge, D. R. (2005) Human Sco1 and Sco2 function as copper-binding proteins, J. Biol. Chem. 280, 34113-34122.
- [52] Siluvai, G. S., Nakano, M., Mayfield, M., and Blackburn, N. J. (2011) The essential role of the Cu (II) state of Sco in the maturation of the CuA center of cytochrome oxidase: evidence from H135Met and H135SeM variants of the Bacillus subtilis Sco, J. Biol. Inorg. Chem. 16, 285-297.
- [53] Siluvai, G. S., Nakano, M. M., Mayfield, M., Nilges, M. J., and Blackburn, N. J. (2009) H135A controls the redox activity of the Sco copper center. Kinetic and spectroscopic studies of the His135Ala variant of Bacillus subtilis Sco, *Biochemistry 48*, 12133-12144.
- [54] Abriata, L. A., Banci, L., Bertini, I., Ciofi-Baffoni, S., Gkazonis, P., Spyroulias, G. A., Vila, A. J., and Wang, S. (2008) Mechanism of CuA assembly, *Nat. Chem. Biol. 4*, 599-601.
- [55] Siluvai, G. S., Mayfield, M., Nilges, M. J., DeBeer George, S., and Blackburn, N. J. (2010) Anatomy of a red copper center: spectroscopic identification and reactivity of the copper centers of Bacillus subtilis Sco and its Cys-to-Ala variants, *J. Am. Chem. Soc. 132*, 5215-5226.
- [56] Chacón, K. N., and Blackburn, N. J. (2012) Stable Cu (II) and Cu (I) mononuclear intermediates in the assembly of the CuA center of Thermus thermophilus cytochrome oxidase, *J. Am. Chem. Soc.* 134, 16401-16412.
- [57] Ghosh, M. K., Basak, P., and Mazumdar, S. (2013) Mechanism of Copper Incorporation in Subunit II of Cytochrome c Oxidase from Thermus thermophilus: Identification of Intermediate Species, *Biochemistry* 52, 4620-4635.
- [58] Wang, X., Ang, M. C., and Lu, Y. (1999) Kinetics of Copper Incorporation into an Engineered Purple Azurin, *J. Am. Chem. Soc.* 121, 2947-2948.
- [59] Wilson, T. D., Savelieff, M. G., Nilges, M. J., Marshall, N. M., and Lu, Y. (2011) Kinetics of Copper Incorporation into a Biosynthetic Purple CuA Azurin: Characterization of Red, Blue, and a New Intermediate Species, J. Am. Chem. Soc. 133, 20778-20792.
- [60] Farrar, J. A., Formicka, G., Zeppezauer, M., and Thomson, A. J. (1996) Magnetic and optical properties of copper-substituted alcohol dehydrogenase: a bisthiolate copper(II) complex, *Biochem. J.* 317, 447-456.

- [61] Maret, W., Dietrich, H., Ruf, H.-H., and Zeppezauer, M. (1980) Active Site-Specifc Reconstituted Copper (II) Horse Liver Alcohol Dehydrogenase: A Biological Model for Type 1 Cu2+ and its Changes Upon Ligand Binding and Confirmational Transitions, *J. Inorg. Biochem.* 12, 241-252.
- [62] Maret, W., and Kozlowski, H. (1987) Biochim. Biophys. Acta. 912, 329.
- [63] Robinson, H., Ang, M. C., Gao, Y.-G., Hay, M. T., Lu, Y., and Wang, A. H. J. (1999) Structural Basis of Electron Transfer Modulation in the Purple CuA Center, *Biochemistry 38*, 5677-5683.
- [64] Nilges, M. J., Matteson, K., and Belford, R. L. (2006) SIMPOW6: A software package for the simulation of ESR powder-type spectra. In ESR Spectroscopy in Membrane Biophysics; Hemminga, M. A., Berliner, L., Eds., Vol. 27, Springer, New York.
- [65] George, G. N., Laboratory:, S. S. R., and Menlo Park, C., 1995. (1995) EXAFSPAK, Stanford Synchrotron Radiation Laboratory:, Menlo Park, CA.
- [66] Gurman, S., Binsted, N., and Ross, I. (1986) A rapid, exact, curved-wave theory for EXAFS calculations. II. The multiple-scattering contributions, *J. Phys. C: Solid State Phys.* 19, 1845.
- [67] Ramachandran, G. N., Ramakrishnan, C., and Sasisekharan, V. (1963) Stereochemistry of polypeptide chain configurations, *J. Mol. Biol.* 7, 95-99.
- [68] Ghosh, M. K., Rajbongshi, J., Basumatary, D., and Mazumdar, S. (2012) Role of the Surface-Exposed Leucine 155 in the Metal Ion Binding Loop of the CuA Domain of Cytochrome c Oxidase from Thermus thermophilus on the Function and Stability of the Protein, *Biochemistry* 51, 2443-2452.
- [69] Solomon, E. I., Szilagyi, R. K., DeBeer George, S., and Basumallick, L. (2004) Electronic Structures of Metal Sites in Proteins and Models: Contributions to Function in Blue Copper Proteins, Chem. Rev. 104, 419-458.

Table of Contents Graphic

